Observation and characterization of cavity Rydberg polaritons

Jia Ningyuan, Alexandros Georgakopoulos, Albert Ryou, Nathan Schine, Ariel Sommer, and Jonathan Simon

Phys. Rev. A **93**, 041802 — Published 13 April 2016

DOI: 10.1103/PhysRevA.93.041802

Observation and Characterization of Cavity Rydberg Polaritons

Jia Ningyuan,[1] Alexandros Georgakopoulos,[1] Albert Ryou,[1] Nathan Schine,[1] Ariel Sommer,[1] and Jonathan Simon[1]

[1] *Department of Physics and James Franck Institute, University of Chicago, Chicago, IL*

We experimentally demonstrate the emergence of a robust quasi-particle, the cavity Rydberg polariton, when an optical cavity photon hybridizes with a collective Rydberg excitation of a laser-cooled atomic ensemble. Free-space Rydberg polaritons have recently drawn intense interest as tools for quantum information processing and few-body quantum science. Here we explore the properties of their cavity counterparts in the single-particle sector, observing an enhanced lifetime and slowed dynamics characteristic of cavity dark polaritons. We measure the range of cavity frequencies over which the polaritons persist, corresponding to the spectral width available for polariton quantum dynamics, and the speed limit for quantum information processing. Further, we observe a cavity-induced suppression of inhomogeneous broadening channels and demonstrate the formation of Rydberg polaritons in a multimode cavity. In conjunction with recent demonstrations of Rydberg-induced cavity nonlinearities, our results point the way towards using cavity Rydberg polaritons as a platform for creating high fidelity photonic quantum materials and, more broadly, indicate that cavity dark polaritons offer enhanced stability and control uniquely suited to optical quantum information processing applications beyond the Rydberg paradigm.

PACS numbers: 42.50.Gy, 42.50.Pq, 32.80.Ee, 71.36.+c

Engineered quasi-particles are a powerful tool for many-body physics and quantum information science, providing the opportunity to build particles imbued with properties chosen from multiple constituent systems. Photonic quasi-particles are particularly appealing, as optical structures can control their propagation, and they can be read out and transmitted over long distances. Examples include exciton polaritons in semiconductor microcavities [1–3], whose mass and trapping arise from a photonic component, and mean-field interactions from an excitonic component; magnon-polaritons [4–6], providing long-lived storage of quantum information in a collective atomic hyperfine excitation; and surface plasmon polaritons [7], where the photonic component provides tight confinement, and thus strong interactions due to hybridization with a single emitter.

The Rydberg polariton [8–19] has recently emerged as a particularly interesting photonic quasiparticle for non-linear quantum optics; its Rydberg component provides interactions that are strong at the single-quantum level, enabling single-photon transistors for quantum information processing [20–22], while its photonic component allows interfacing to quantum communication channels [23]. While these particles have been primarily studied in free-space, trapping the photonic component in an optical resonator enhances interactions between polaritons [14, 24], and promises exquisite control of polariton dispersion [25] necessary to induce photonic BECs [1, 26], emergent crystallinity [27–31], and topological fluids in synthetic magnetic fields [27, 32–36].

In this Rapid Communication, we observe the cavity Rydberg polariton and characterize its single-body properties, many of which apply to all cavity dark polaritons. We first explore the dark-polariton spectrum, quantitatively demonstrating compression [38, 39] compared to the bare cavity spectrum near EIT resonance, corresponding to a slowdown of dynamics. We investigate the available bandwidth for many-body physics or quantum information processing (QIP) set by the width of the EIT resonance versus the cavity frequency, and demon-

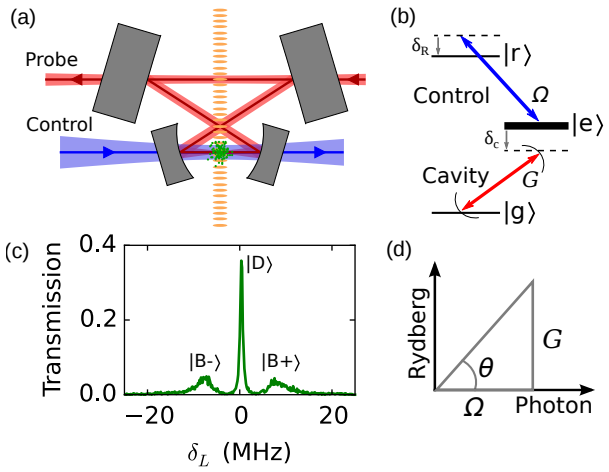

FIG. 1. (Color online) Cavity Rydberg EIT. (a) Schematic of the experimental setup, showing the ^{87}Rb atomic sample in the waist of a running-wave cavity after being transported by a moving optical lattice. The cavity mirrors are high finesse at the probe wavelength (780 nm), and AR coated for the control laser (480 nm) that counter-propagates through the sample. (b) Level diagram showing that the cavity mode couples the atomic ground state to an excited state, with collective vacuum Rabi frequency G and detuning δ_c, while the control laser couples the excited state to a Rydberg level, with Rabi frequency Ω and detuning δ_R. (c) Transmission spectrum as a fraction of the peak empty-cavity transmission showing peaks due to the cavity Rydberg dark polariton $|D\rangle$ and two bright polaritons $|B\pm\rangle$. Here G=13 MHz, Ω=7 MHz, $\delta_c = \delta_R = 0$. (d) Decomposition of the dark polariton into cavity photon and Rydberg components, set by the couplings G and Ω that define the dark state rotation angle θ.

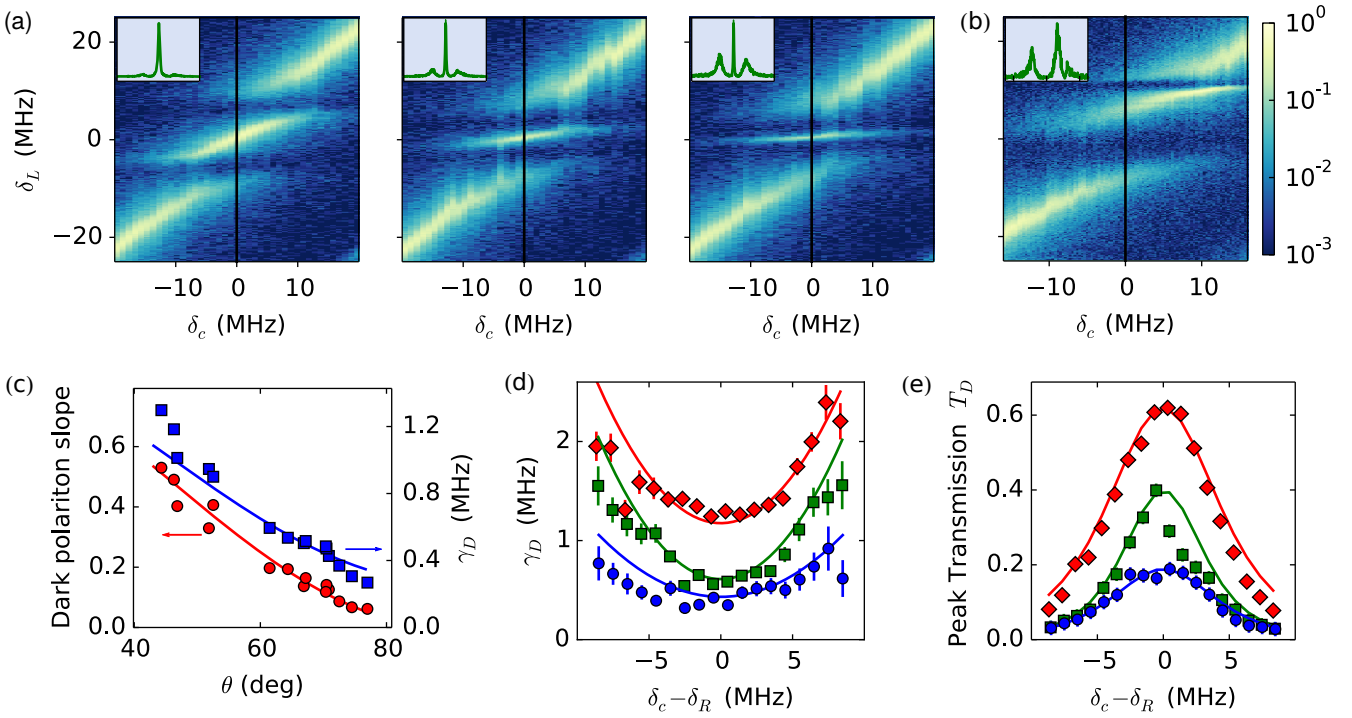

FIG. 2. (Color online) Spectroscopy of cavity Rydberg polaritons. (a) Cavity transmission spectra as a function of cavity detuning δ_c for several values of the control laser power. From left to right, θ (deg)=43, 62, 72; Ω= 13.1(1), 6.9(1), 4.9(1) MHz; G = 12.3(2), 13.0(1), 14.7(1) MHz. Here $|\delta_R| < 1$ MHz. Insets in (a) and (b): spectra along the vertical line at $\delta_c = 0$. Color scale for (a) and (b): cavity transmission as a fraction of the empty-cavity peak transmission. (b) Transmission spectrum at non-zero control laser detuning δ_R = 9.8(4) MHz. Here Ω = 8.2(6) MHz, G = 16.8(3) MHz. (c) Energy and lifetime versus dark state rotation angle. Red circles (left): dark polariton slope $d\delta_D/d\delta_c$. Blue squares (right): dark polariton inverse lifetime γ_D. Solid lines: theoretical predictions, using Ω obtained from the calibrated control laser power and G obtained from fitting to the transmission spectrum. (d) and (e) show the effect of detuning the cavity from EIT resonance using the data in (a). Correspondence to (a): left–diamonds (red), middle–squares (green), right–circles (blue).(d) γ_D versus cavity detuning from EIT resonance. Solid lines: second-order prediction (1), using γ_R and G obtained from the transmission spectrum at $\delta_R - \delta_c$=0. (e) Height T_D of the dark polariton peak versus cavity detuning. Solid lines: theoretical prediction using (2) plus higher order corrections [37] that are only significant for the lower (blue) curve.

strate the connection to the free-space EIT linewidth. We then observe a novel suppression of inhomogeneous broadening channels and provide a quantitative model for this effect. Finally, we explore dark-polariton physics in a multimode regime with an eye towards few-particle quantum material and QIP experiments.

Our system consists of an ensemble of ground-state atoms in the waist of an optical cavity, as illustrated in Fig. 1(a). A cavity photon ($|c\rangle$) may be absorbed by the atomic ensemble, generating a collective excitation $|e_c\rangle$ of the $|e\rangle$ level, with collective vacuum Rabi frequency G. A control laser transfers the $|e_c\rangle$ state to a collective excitation $|r_c\rangle$ of the Rydberg level $|r\rangle$ with Rabi frequency Ω. The eigenstates of the coupled atom-cavity system include a dark state $|D\rangle$ and two bright states $|B\pm\rangle$. When the cavity is tuned to the EIT resonance condition $\delta_c = \delta_R$, with δ_c the frequency of the cavity mode minus the atomic transition frequency and δ_R the transition frequency from $|e\rangle$ to $|r\rangle$ minus the frequency of the control laser, the dark state is $|D\rangle = \cos\theta\,|c\rangle - \sin\theta\,|r_c\rangle$, where $\theta \equiv \tan^{-1}(G/\Omega)$ is the dark state rotation angle [9, 40]. We study the dark polariton energy $\hbar\delta_D$ (relative to the atomic resonance) and inverse lifetime γ_D by observing the transmission spectrum in cavity Rydberg EIT.

Experiments begin with a laser-cooled ^{87}Rb atomic sample that we optically transport into the waist of a running-wave bow-tie optical cavity. The cavity is tuned near the atomic D_2 transition (780 nm) from the $|g\rangle = 5S_{1/2}(F{=}2)$ ground state to the $|e\rangle = 5P_{3/2}(F{=}3)$ excited state. The control laser (wavelength 480 nm, waist 29 μm) that couples to the $|r\rangle = nS_{1/2}$ Rydberg level counter-propagates through the sample. Here we use primarily $n = 40$. At 780 nm, the cavity has a TEM_{00} mode waist of 12 μm × 11 μm ($1/e^2$ intensity radii) between the lower mirrors, and a finesse of 2500 (1.8 MHz FWHM linewidth). We obtain transmission spectra by sweeping the detuning δ_L of a probe laser (laser frequency minus the atomic transition frequency) linearly over 1

ms and detecting the transmitted light with a single-photon counter. By using sufficiently low principle quantum numbers and photon densities, we work in a regime of small polariton-polariton interactions and isolate the properties of individual polaritons.

Because the polariton spends much of its time as a collective Rydberg excitation rather than a resonator photon, polariton dynamics are expected to be proportionally slower than those of their photonic constituent [38, 39]. We explore this effect in Figure 2(a)-(c), where we measure the resonator spectrum as a function of cavity frequency (within each frame of (a)), for several dark state rotation angles (different frames of (a)). The energy of the dark polariton tunes more slowly than the cavity itself by a factor set by the dark-state rotation angle, as shown in Figure 2(c), in quantitative agreement with the first-order expansion [37, 38]: $\delta_D \approx \delta_c \cos^2\theta + \delta_R \sin^2\theta$.

The utility of polaritons depends on their lifetime: strong single-photon nonlinearities require an interaction energy [27] greater than the width of the polariton resonance, and photonic materials require stable polaritons to allow well-resolved many-body states [34]. The primary loss channels for dark polaritons are outcoupling of their photonic component through the cavity and decay of the Rydberg excitation, giving $\gamma_D \approx \kappa \cos^2\theta + \gamma_R \sin^2\theta$ at EIT resonance [37, 38]. The right axis in Fig. 2(c) shows γ_D obtained from the full-width at half-maximum of a Lorentzian fit to the dark polariton peak with the cavity at EIT resonance, compared to theory; it reaches a minimum of 0.26(1) MHz, significantly less than the bare cavity linewidth of 1.8 MHz.

Polariton interactions, as well as spatial dynamics in multimode cavities, would lead to a detuning from EIT resonance. This detuning introduces a fundamental loss channel that has not been explored in previous experimental studies of (ground state) cavity EIT [39, 41–45]. Figure 2(d) shows the dependence of polariton linewidth on detuning from EIT resonance, in quantitative agreement with a simple model [37, 38]:

$$\gamma_D \approx \kappa \cos^2\theta + \gamma_R \sin^2\theta + a\,(\delta_c - \delta_R)^2 \qquad (1)$$

with $a \equiv 4\Omega^2 G^2 \Gamma/(\Omega^2 + G^2)^3$ giving the strength of the (previously unreported) quadratic term. The cavity detuning required to double the polariton decay rate is $\delta_c - \delta_R = \Delta \equiv \frac{1}{2}\frac{\Omega^2/\Gamma}{\sqrt{OD}}/\cos^2\theta$ for $\gamma_R \ll \kappa$, where $OD \equiv \frac{G^2}{\kappa\Gamma}$ is the cavity-enhanced optical depth. When the cavity is detuned by Δ, the dark polariton energy moves only by $\Delta \times \cos^2\theta = \frac{1}{2}\frac{\Omega^2/\Gamma}{\sqrt{OD}}$, which is identical to the free-space EIT linewidth [40].

The cavity EIT bandwidth is also observable in the height (maximum transmission) of the dark polariton resonance. We explore this behavior in Fig. 2(e), and observe that the peak transmission follows a squared Lorentzian [37]:

$$T_D \propto \left[1 + (\delta_c - \delta_R)^2/(\Gamma_w/2)^2\right]^{-2} \qquad (2)$$

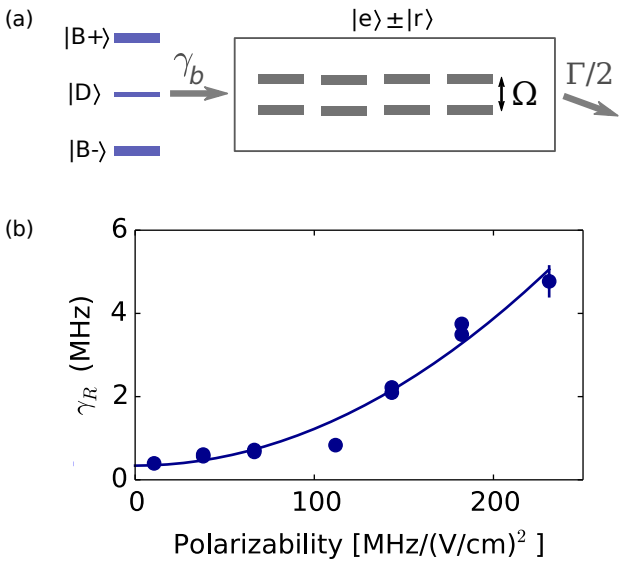

FIG. 3. (Color online) Collective suppression of decoherence. (a) Inhomogeneous broadening couples the dark polariton to a bath of states orthogonal to the cavity mode. The splitting from the control laser detunes these states from the dark state, suppressing the lossy channel. (b) Effective decay rate γ_R of the collective Rydberg state for varying principle quantum number n versus the polarizability of the Rydberg state. Here n=40, 48, 52, 56, 58, 60, and 62. Ω (MHz)=7.8(5), G (MHz) = 12(2), average and std. dev. over the data sets. Solid line: quadratic fit.

with $\Gamma_w \approx 2\Delta$ as defined above. The cavity EIT width Γ_w determines the bandwidth available for polariton dynamics and interactions. In a multimode cavity, Γ_w sets the maximum polariton kinetic energy transverse to the cavity. In a quantum gate based on detuning from EIT resonance [8], the maximum detuning sets a limit on the gate time of $\sim 1/\Gamma_w$.

Compared to ground-state cavity polaritons, Rydberg cavity polaritons exhibit an enhanced sensitivity to inhomogeneous broadening of the collective atomic excitation arising from the Doppler effect (due to the wavelength mismatch in the ladder configuration) and inhomogeneous electric fields (due to the large polarizability of Rydberg atoms). The latter is particularly significant near surfaces [46–48] such as the dielectric mirrors of an optical cavity.

Because these decoherence channels enter the polariton linewidth in parametrically similar ways [37], we explore the dephasing due to an electric field gradient where we have direct control over single-particle broadening by changing principle quantum number n of the Rydberg state, and thereby the Rydberg polarizability $\alpha_n \propto n^7$. Figure 3(b) shows the loss rate γ_R of $|r_c\rangle$ versus α_n, obtained by fitting the measured spectra. For spectroscopy of completely independent atoms, γ_R would vary in proportion to the inhomogeneous broadening $\gamma_b \propto \alpha_n$ of the Rydberg level. However, the data in Fig. 3(b) vary

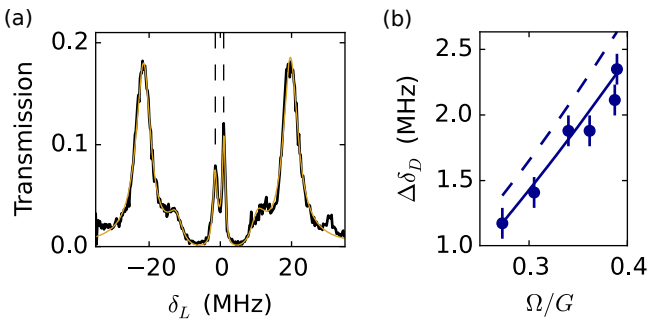

FIG. 4. (Color online) Rydberg polaritons in two cavity modes. The TEM_{02} and TEM_{10} modes are tuned to ±10 MHz from EIT resonance. (a) Transmission spectrum for Ω/G=0.39, with $G = 27$ MHz. The dark polariton resonances (dashed lines) are separated by $\Delta\delta_D = 2.3$ MHz. Curve: fit to theoretical model for two orthogonal collective states. (b) Adjusting the control laser power varies the photonic component of the dark polariton states, tuning $\Delta\delta_D$. Dashed curve: first-order prediction. Solid curve: numerical solution.

quadratically with α_n. This suppression of decoherence arises because dephasing couples the collective Rydberg state $|r_c\rangle$ to a bath of collective excitations [49] of the hybridized $|r\rangle$ and $|e\rangle$ levels, that, in turn, have no coupling to the cavity mode. In the rotating frame, these states are detuned by $\pm\Omega/2$ relative to the dark polariton (Fig. 3a); For $\gamma_b < \Gamma, \Omega$, this detuning leads to a suppressed loss rate of $s_b\gamma_b^2\Gamma/\Omega^2$ from $|r_c\rangle$; numerical simulations [37] reveal that $s_b \approx 4$, for a normal distribution of Stark shifts with standard deviation γ_b. The simulations confirm that Doppler decoherence is similarly suppressed, and that while inhomogeneous control-field coupling does renormalize $|r_c\rangle$, a dark state exists [37] which is negligibly broadened by the inhomogeneous coupling.

The suppression of decoherence arising from inhomogeneous broadening does not depend on using Rydberg states, and therefore also applies to ground state polaritons. In particular, it can be used to improve the coherence time of spin waves in DLCZ [23]-style single-photon source experiments [4–6]. Here, we point out that the presence of the control field allows the spin-wave to continuously refresh itself, suppressing the decoherence that would otherwise be present; indeed, we predict a parameter regime in which the spin-wave lives longer in the presence of the read-out field [37].

To employ cavity polaritons in quantum materials, it is essential to harness multiple cavity modes simultaneously. The different cavity modes correspond to the single polariton spatial eigenstates resulting from motional dynamics in harmonic traps or photonic Landau levels [25, 27, 36]. For quantum information processing, the different modes can be used to implement one [50] or more [51] qubits. Here we demonstrate, for the first time, Rydberg EIT in two cavity modes.

Our experimental cavity is designed such that the TEM_{02} and TEM_{10} modes are nearly degenerate, with a separation of $\Delta\delta_c = 20$ MHz, while the TEM_{00} mode is isolated [37]. This mode spectrum allows us to switch seemlessly between single-mode EIT physics in the TEM_{00} mode and multimode physics in the TEM_{02} and TEM_{10} manifold by tuning the cavity length. To demonstrate dark polaritons in two modes, we tune the TEM_{02} and TEM_{10} modes to either side of the atomic resonance. We align the probe beam to couple to both modes, and collect the transmitted light in a multimode fiber. Figure 4(a) shows a measured transmission spectrum for two-mode cavity Rydberg EIT. The two central peaks are dark polaritons in the two modes and are separated by much less than 20 MHz due to strong light-matter mixing. Because the atomic density is approximately uniform across the cavity waist, the cavity modes do not mix, and polaritons form independently in the two modes [37]. The frequencies of the two dark polariton resonances can then be predicted by considering each mode separately, using the results demonstrated in Fig. 2. In particular, we show in Fig. 4(b) that the splitting $\Delta\delta_D$ between the two dark polariton peaks tunes with the dark state rotation angle as $\Delta\delta_D \approx \Delta\delta_c \cos^2\theta$, plus higher-order corrections in $\Delta\delta_c$. The direct relation between the dark polariton spectrum and the underlying cavity spectrum implies that dark polaritons inherit the dynamics of the cavity modes within the bandwidth Γ_w, and up to a slowing of timescales by $\cos^2\theta$. Therefore, dark polaritons in multimode cavities inherit the mass, trapping, and effective magnetic field of their photonic constituents [25, 27, 36].

In conclusion, we have observed Rydberg polaritons in an optical cavity and studied their energy and coherence properties; we demonstrate that the available bandwidth for polariton dynamics and interactions is closely related to the free-space EIT linewidth, and reveal a collective suppression of inhomogeneous decoherence. Introducing polariton-polariton interactions by working with higher Rydberg levels will provide a way to extend single photon source [12, 13] and single photon transistor [20–22] technology to higher fidelity via an optical cavity. Introduction of near-degenerate multimode cavities [25, 27] will provide a spatial degree of freedom for exploring exotic condensed-matter models using Rydberg polaritons.

ACKNOWLEDGMENTS

The authors thank Lindsay Bassman, Graham Greve, Aaron Krahn, Sohini Upadhyay, Jin Woo Sung, Michael Cervia, and William Tahoe Schrader for contributions to the experimental system. The U.S. AFOSR (grant FP053419-01-PR) supported apparatus construction and the U.S. DOE (grant FP054241-01-PR) supported theoretical modeling, as well as data-collection and analysis.

[1] R. Balili, V. Hartwell, D. Snoke, L. Pfeiffer, and K. West, Science **316**, 1007 (2007).
[2] H. Deng, H. Haug, and Y. Yamamoto, Rev. Mod. Phys. **82**, 1489 (2010).
[3] I. Carusotto and C. Ciuti, Rev. Mod. Phys. **85**, 299 (2013).
[4] C. W. Chou, S. V. Polyakov, A. Kuzmich, and H. J. Kimble, Phys. Rev. Lett. **92**, 213601 (2004).
[5] T. Chanelière, D. N. Matsukevich, S. D. Jenkins, S.-Y. Lan, T. a. B. Kennedy, and A. Kuzmich, Nature **438**, 833 (2005).
[6] J. Simon, H. Tanji, J. K. Thompson, and V. Vuletić, Phys. Rev. Lett. **98**, 183601 (2007).
[7] A. V. Akimov, A. Mukherjee, C. L. Yu, D. E. Chang, A. S. Zibrov, P. R. Hemmer, H. Park, and M. D. Lukin, Nature **450**, 402 (2007).
[8] M. D. Lukin, M. Fleischhauer, R. Cote, L. M. Duan, D. Jaksch, J. I. Cirac, and P. Zoller, Phys. Rev. Lett. **87**, 037901 (2001).
[9] M. D. Lukin, Rev. Mod. Phys. **75**, 457 (2003).
[10] J. D. Pritchard, D. Maxwell, A. Gauguet, K. J. Weatherill, M. P. A. Jones, and C. S. Adams, Phys. Rev. Lett. **105**, 193603 (2010).
[11] A. V. Gorshkov, J. Otterbach, M. Fleischhauer, T. Pohl, and M. D. Lukin, Phys. Rev. Lett. **107**, 133602 (2011).
[12] Y. O. Dudin and A. Kuzmich, Science **336**, 887 (2012).
[13] T. Peyronel, O. Firstenberg, Q. Y. Liang, S. Hofferberth, A. V. Gorshkov, T. Pohl, M. D. Lukin, and V. Vuletić, Nature **488**, 57 (2012).
[14] V. Parigi, E. Bimbard, J. Stanojevic, A. J. Hilliard, F. Nogrette, R. Tualle-Brouri, A. Ourjoumtsev, and P. Grangier, Phys. Rev. Lett. **109**, 233602 (2012).
[15] J. Stanojevic, V. Parigi, E. Bimbard, A. Ourjoumtsev, and P. Grangier, Phys. Rev. A **88**, 053845 (2013).
[16] D. Maxwell, D. J. Szwer, D. Paredes-Barato, H. Busche, J. D. Pritchard, A. Gauguet, K. J. Weatherill, M. P. A. Jones, and C. S. Adams, Phys. Rev. Lett. **110**, 103001 (2013).
[17] C. S. Hofmann, G. Günter, H. Schempp, M. Robert-de-Saint-Vincent, M. Gärttner, J. Evers, S. Whitlock, and M. Weidemüller, Phys. Rev. Lett. **110**, 203601 (2013).
[18] O. Firstenberg, T. Peyronel, Q. Y. Liang, A. V. Gorshkov, M. D. Lukin, and V. Vuletić, Nature **502**, 71 (2013).
[19] P. Bienias, S. Choi, O. Firstenberg, M. F. Maghrebi, M. Gullans, M. D. Lukin, A. V. Gorshkov, and H. P. Büchler, Phys. Rev. A **90**, 053804 (2014).
[20] H. Gorniaczyk, C. Tresp, J. Schmidt, H. Fedder, and S. Hofferberth, Phys. Rev. Lett. **113**, 053601 (2014).
[21] S. Baur, D. Tiarks, G. Rempe, and S. Dürr, Phys. Rev. Lett. **112**, 073901 (2014).
[22] D. Tiarks, S. Baur, K. Schneider, S. Dürr, and G. Rempe, Phys. Rev. Lett. **113**, 053602 (2014).
[23] L.-M. Duan, M. D. Lukin, J. I. Cirac, and P. Zoller, Nature **414**, 413 (2001).
[24] R. Boddeda, I. Usmani, E. Bimbard, A. Grankin, A. Ourjoumtsev, E. Brion, and P. Grangier, arXiv:1512.08480 [cond-mat, physics:physics, physics:quant-ph] (2015).
[25] A. Sommer and J. Simon, arXiv:1511.00595 [cond-mat, physics:physics, physics:quant-ph] (2015).
[26] J. Klaers, J. Schmitt, F. Vewinger, and M. Weitz, Nature **468**, 545 (2010).
[27] A. Sommer, H. P. Büchler, and J. Simon, arXiv:1506.00341 [cond-mat.quant-gas] (2015).
[28] D. E. Chang, V. Gritsev, G. Morigi, V. Vuletić, M. D. Lukin, and E. A. Demler, Nature Phys. **4**, 884 (2008).
[29] S. Gopalakrishnan, B. L. Lev, and P. M. Goldbart, Nature Phys. **5**, 845 (2009).
[30] J. Otterbach, M. Moos, D. Muth, and M. Fleischhauer, Phys. Rev. Lett. **111**, 113001 (2013).
[31] A. J. Kollár, A. T. Papageorge, K. Baumann, M. A. Armen, and B. L. Lev, New. J Phys. **17**, 043012 (2015).
[32] F. Grusdt and M. Fleischhauer, Phys. Rev. A **87**, 043628 (2013).
[33] M. Hafezi, M. D. Lukin, and J. M. Taylor, New J. Phys. **15**, 063001 (2013).
[34] R. O. Umucalılar, M. Wouters, and I. Carusotto, Phys. Rev. A **89**, 023803 (2014).
[35] M. F. Maghrebi, N. Y. Yao, M. Hafezi, T. Pohl, O. Firstenberg, and A. V. Gorshkov, Phys. Rev. A **91**, 033838 (2015).
[36] N. Schine, A. Ryou, A. Gromov, A. Sommer, and J. Simon, arXiv:1511.07381 [cond-mat.quant-gas] (2015).
[37] See Supplemental Material at http:// for additional details on the experimental implementation, theoretical description, and numerical simulations.
[38] M. D. Lukin, M. Fleischhauer, M. O. Scully, and V. L. Velichansky, Opt. Lett **23**, 295 (1998).
[39] G. Hernandez, J. Zhang, and Y. Zhu, Phys. Rev. A **76**, 053814 (2007).
[40] M. Fleischhauer, A. Imamoglu, and J. P. Marangos, Rev. Mod. Phys. **77**, 633 (2005).
[41] G. Müller, M. Müller, A. Wicht, R.-H. Rinkleff, and K. Danzmann, Phys. Rev. A **56**, 2385 (1997).
[42] H. Wang, D. J. Goorskey, W. H. Burkett, and M. Xiao, Opt. Lett **25**, 1732 (2000).
[43] H. Wu, J. Gea-Banacloche, and M. Xiao, Phys. Rev. Lett. **100**, 173602 (2008).
[44] M. Mücke, E. Figueroa, J. Bochmann, C. Hahn, K. Murr, S. Ritter, C. J. Villas-Boas, and G. Rempe, Nature **465**, 755 (2010).
[45] T. Kampschulte, W. Alt, S. Manz, M. Martinez-Dorantes, R. Reimann, S. Yoon, D. Meschede, M. Bienert, and G. Morigi, Phys. Rev. A **89**, 033404 (2014).
[46] A. Tauschinsky, R. M. T. Thijssen, S. Whitlock, H. B. van Linden van den Heuvell, and R. J. C. Spreeuw, Phys. Rev. A **81**, 063411 (2010).
[47] H. Hattermann, M. Mack, F. Karlewski, F. Jessen, D. Cano, and J. Fortágh, Phys. Rev. A **86**, 022511 (2012).
[48] S. D. Hogan, J. A. Agner, F. Merkt, T. Thiele, S. Filipp, and A. Wallraff, Phys. Rev. Lett. **108**, 063004 (2012).
[49] J. Honer, R. Löw, H. Weimer, T. Pfau, and H. P. Büchler, Phys. Rev. Lett. **107**, 093601 (2011).
[50] Z.-S. Yuan, Y.-A. Chen, B. Zhao, S. Chen, J. Schmiedmayer, and J.-W. Pan, Nature **454**, 1098 (2008).
[51] A. Grodecka-Grad, E. Zeuthen, and A. S. Sørensen, Phys. Rev. Lett. **109**, 133601 (2012).